Supplemental Data

Insights into Hsp70 Chaperone Activity from a Structure of the Yeast Hsp110 Sse1

Qinglian Liu and Wayne A. Hendrickson

Supplemental Text S1

Proteolytic susceptibility

Full-length Sse1(2-693) could be cleaved by trypsin, and products were identified from N-terminal sequencing and mass spectrometry. In the presence of ATP, cleavage occurred both after Arg388 to give a ~40kD N-terminal half and a C-terminal half (389-693), and also after either Arg654 or Arg673 at the C-terminus to give the 389-673 and 389-654 products. An unresolved, near full-length ~70kD band had an intact N-terminus but presumably containing 2-654 and 2-673 fragments as well as the full-length protein.

Subsequently, we also analyzed the limited trypsinolysis of Sse1(2-659) as a function of nucleotide state. A representative result is shown in Fig. S10. In the presence of ATP, much of the Sse1(2-659) protein remains uncleaved, and there are two major cleaved bands, at ~40kD and at ~30kD. N-terminal sequencing showed that the 40kD band starts from the N-terminus and that the 30kD band starts with VRPFKFE (i.e. cleavage after Arg388). The molecular size by mass spectrometry for the 40kD band is 42754 Daltons (42739 from a separate experiment). The 30 kD band proved to contain two fragments by mass spectrometry, giving masses of 31131 and 30657 Daltons (31096 and 30551 from a separate run). Combining N-termini and masses calculated from the sequence, we identify the fragment expanses as 2-388 for the N-terminal fragment (42733.6 Daltons) and 389-654 and 389-659 for the C-terminal fragments (30429.1 and 30972.7 Daltons, respectively).

In the presence of ADP, only the 30kD band and a ~60kD band (doublet at better separation) were observed. Based on N-terminal sequencing, the 60kD band comprises two N-termini corresponding to cleavages after Arg70 (ΔN70) and Arg105 (ΔN105). The 30kD band contains the same 389-654 and 389-659 products as with ATP. Consistent with susceptibility at Arg105 in ADP, the ~30kD band cleaved in ADP from full-length Sse1(2-693) also contains a small amount of 106-388. The ~40kD NBD band expected from cleavage after Arg388 was completely digested to oligopeptides, as also happened upon digestion of full-length Sse1(2-693) in ADP. Digestion profiles in the presence of AMP-PNP are essentially indistinguishable from those in ADP, but digestion in the absence of any nucleotide gave a rather different pattern with more digestion products.

Supplemental Text S2

Structure determination and analysis

Crystals were obtained initially for full-length Sse1 protein in the presence of ATP/Mg^{2+}/K^{+}, equally well from Sse1(-1-693) and Sse1(2-693); however, none of these diffracted beyond 7.5Å spacings. A construct, Sse1(2-659), shortened C-terminally (Δ34) as in the C-terminal truncation used in structural analysis of the SBD portion of DnaK (Zhu et al., 1996), was then made and this crystallized well. The even further shortened Sse1(Δ44) is fully functional in yeast (Shaner et al., 2004). Subsequent proteolytic analysis of full-

length Sse1 showed a natural susceptibility to cleavage after Arg654, nearly analogous to the DnaK truncation, thereby corroborating the relevant integrity of Sse1(2-659).

The crystals are in a C2 lattice with a=218.1Å, b=125.3Å, c=74.7Å and β=98.7º, and they contain 64% solvent and two ATP/Mg^{2+}/K^{+} complexes of Sse1 per asymmetric unit. The structure was solved by MAD phasing from selenomethionine-substituted Sse1, and resulting electron density maps were readily interpretable (Fig. S1A). Positioning of ATP was straightforward and the protein density (Fig. S1B) supported automatic interpretation of 1066 residues (81%), which were built by application of Arp/wArp (Perrakis et al., 1999). Another 174 residues were fitted manually. The remaining 74 were too disordered to model, and another 43 of the fitted residues had insufficient density to model beyond Cβ (17 in protomer A and 26 in protomer B). The experimental maps compare favorably with (2|Fo| -|Fc|) maps (Figs. S1B) after refinement at 2.4Å resolution to an *R*-value of 19.5% (R_{free} = 23.5%). The refined model comprises 10,062 atoms and has good stereochemistry with no Ramachandran outliers. Hsp110 insertion segments are disordered and unmodeled in both protomers, as are a few residues from termini and other internal loops (2 in protomer A; 1 in B) (Fig. S2).

The Sse1 dimer has an elongated diamond-like shape (Fig. 1B), which arises from extended α-helical lid subdomains interacting with NBDs of partner protomers. SBD-distal tips of the NBDs interact at the dimeric center, whereas SBD-proximal bases of the NBDs associate with widely separated SBD β-subdomains at acute opposites of the diamond. Protomer B has somewhat better order than A, so we use it in our analyses.

The two subunits in the asymmetric unit of the crystal were built independently, and for the most part automatically, and they were refined without symmetry restraints. Therefore, deviations between the two protomers can be taken as a measure of structural precision and systematic overall differences are likely to be real. A superposition of the two protomers based on Cα positions shows that the dimer is nearly diad symmetric (χ=179.6º, t_χ=0.59Å). Overall, r.m.s. deviations between the protomers are 0.43Å for Cα positions and 0.65Å for all atoms. Protomers in the dimer behave essentially as rigid bodies; thus, individual transformations that relate subdomains are all nearly the same and r.m.s.d.s from these individual superpositions (Table S1) are little different from those within the overall superposition. Deviations are the lowest within NBD and the greatest within SBD. Protomer A has uniformly greater mobility (<B>=57.8$Å^2$) than in protomer B (<B>=47.9$Å^2$).

The surface features of Sse1 are instructive. We mapped the conservation of sequence onto the molecular surface of NBD (Figs. 5A-C), and we also examined the conservation of SBD surfaces. These mappings were done with the ConSurf program (Landau et al., 2005). We also mapped the interfaces of contact between NBD and SBD, and those of SBD onto NBD are shown in Fig. 5D-F. Finally, we constructed the Grasp (Nicholls et al., 1991) electrostatic-potential surfaces of Sse1 and compared them to those in hHsp70 and DnaK. The electrostatic potential is mapped onto surfaces of Sse1 NBD in Fig. S11A and onto the partner SBD surfaces, viewed from the reverse side, in Fig. S11B. The obligate charge complementarity is evident. Mappings onto the NDB surfaces from hHsp70 and DnaK are shown in Figs. S11 C and D, respectively. It is noteworthy that electrostatic features are not well preserved across Sse1, hHsp70 and DnaK even in regions that have generally high sequence conservation; this may relate to interactions with partner proteins for which specifics are not yet characterized.

Both full-length and Sse1(2-659) were screened for crystallization in the presence of 4 mM ADP in the same buffer as that used with ATP. Crystals were obtained in several conditions similar to those that generated crystals in the presence of ATP. However, none diffracted beyond 10Å except for those from conditions like the ones for our Sse1(ATP) crystals which

diffracted to 2.4Å (0.1M cacodylate-HCl (pH6.5) and 8-10% PEG6000). In this condition, it takes a few days for ATP crystals to grow, but about a month is required for crystallization with ADP. These ADP crystals diffract to the similar range as those ATP crystals. However, upon structure determination, density for ATP was found in the nucleotide-binding pocket instead of ADP.

Supplemental Text S3

Sse1 oligomerization in solution

Sse1(2-659) as purified in the nucleotide-free state (buffered to pH 7.0 in 20 mM Hepes-KOH, 50 mM KCl, and 10mM $Mg(OAc)_2$) eluted from a calibrated size-exclusion column (Superdex 200) at 4ºC in a volume corresponding to a size of about 110kD. Dynamic light scattering experiments, conducted in triplicate in the same buffer as that for size-exclusion chromatography, gave Stokes radii corresponding to 93.4 ± 0.7 kD when nucleotide free, 207.8 ± 1.4 kD when in ADP (4mM), and 229.8 ± 1.1 kD when in ATP (4mM). These results suggest that Sse1 is monomeric when nucleotide free, but that it dimerizes in the presence of nucleotide although more compactly with ADP than with ATP. Equilibrium centrifugation was conducted at varying protein concentrations and different speeds in an effort to estimate the equilibrium constant for dimerization. These experiments were conducted in the same buffer as above but in the presence of ATP (0.5 mM). The resulting profiles could not be fitted by a single association behavior, but separate analyses gave Kd values in the range of 100-200 μM. We suspect that the ATP concentration may not have sufficed at higher protein concentrations, but these observations are consistent with a labile monomer-dimer association for Sse1(ATP).

Supplemental Text S4

A. Comparison of Sse1 to SBD of DnaK

The most complete SBD structure is that from DnaK bound to the heptapeptide NRLLLTG (Zhu et al., 1996); other more truncated Hsp70 SBDs are similar in structure except for instances of C-terminal segments occupying the substrate-binding site (Wang et al., 1998; Morshauser et al., 1999; Stevens et al., 2003; Cupp-Vickery et al., 2004; Jiang et al., 2005). The SBD portion of Sse1 is rearranged radically in comparison, as discussed in the main text. In particular, with β-subdomains of Sse1 and DnaK superimposed (Fig. 2C), the transformation required to superimpose corresponding Cα atoms in αA/αB1 helices is a rotation χ=159.6º and translation t_χ=3.3Å along the axis of rotation. With α-helical lid domains (αB-αE) superimposed (Fig. 2D), a transformation of χ=78.5º and t_χ=-1.1Å is required to superimpose the αA/αB1 helices.

The structure of Sse1(ATP) does not have a bound substrate peptide, but the site comparable to the substrate-binding site in DnaK has properties that seem relevant to the known substrate binding of Hsp110 chaperones. Loops $\mathcal{L}_{1,2}$ and $\mathcal{L}_{3,4}$ form a channel into which the peptide substrate binds in DnaK, with loops $\mathcal{L}_{4,5}$ and $\mathcal{L}_{5,6}$ buttressing on either side. Sse1 in our structure does not have a polypeptide substrate, and its $\mathcal{L}_{1,2}$ and $\mathcal{L}_{3,4}$ loops are pressed against one another. Moreover, these loop lengths are switched in the two structures; $\mathcal{L}_{1,2}$ and $\mathcal{L}_{3,4}$ have three (sequence: M**G**G) and seven (TA**ED**N**Q**S) residues, respectively, in DnaK; whereas they have seven (DK**Q**V**ED**E) and three (T**G**D), respectively, in Sse1. This switch in loop lengths and sequence properties is characteristic for Hsp110s and may relate to putative substrate binding at this site. Likewise, the hydrophobic character of residues contacting the central leucine of the NRLLLTG peptide in the substrate-binding channel of DnaK (Ile401, Thr403, Phe426, Val436 and

Ile438) is also preserved in Sse1 (Tyr404, Trp406, Leu433, Phe439 and Met441) and hHsp110 (Fig. S2). The outer buttressing loop $\mathcal{L}_{5,6}$ is similar in Sse1 as in DnaK, where ordered; but the inner buttressing loop $\mathcal{L}_{4,5}$ of Sse1 is flipped out toward the NBD where it retains the same local tip conformation and packs against β1′-β1 at the SBD N-terminus. The characteristic Hsp110 insertion loop $\mathcal{L}_{7,8}$ is mostly disordered in Sse1.

B. Comparison of Sse1 to NBDs of Hsp70s

Structures of NBDs from bHsc70 and human Hsp70 (hHsp70) in various nucleotide complexes are all essentially the same (Flaherty et al., 1990; Flaherty et al., 1994; Wilbanks and McKay, 1995; O'Brien et al., 1996; Sriram et al., 1997; Johnson and McKay, 1999). Pairwise C_α r.m.s.d.s are within 0.5 Å, both between proteins and in responses to different nucleotides, cations and mutations. NBD structures in NEF complexes (Harrison et al., 1997; Sondermann et al., 2001), or otherwise devoid of nucleotide (Jiang et al., 2005), have subdomain IIB displaced relative to the rest by 13-16º, but otherwise these too are essentially the same as the prototype NBD (Flaherty et al., 1990).

ATP binding does impart conformational changes to intact Hsp70s, but only through NBD-SBD interactions; and these changes are disrupted by even minor perturbations to the nucleotide-binding site (Wilbanks et al., 1995; Johnson and McKay, 1999) and they are not elicited by non-hydrolyzable ATP analogs (Buchberger et al., 1995; Wilbanks et al., 1995).

Although the NBD of Sse1(ATP) is superficially similar to other NBDs, and subdomain topologies are virtually identical, its subdomain dispositions are unprecedented (Fig. 3A). When just adenosine moieties (sandwiched between IIA and IIB) are superimposed, rotations of 22.0, 25.7, 7.7 and 4.1º are required to superimpose the respective subdomains (IA, IB, IIA, IIB) of Sse1 onto hHsp70 as compared with 2.6, 2.8, 2.3 and 3.0º, respectively, for bHsc70 onto hHsp70. The distinction in Sse1 is primarily due to differences at the IA-IIA interface; when IIA subdomains are superimposed, a rotation of 22.1º is needed to superimpose the IA subdomains of Sse1 and hHsp70 whereas IIB mainly rides with IIA (6.5º) and IB mainly rides with IA (4.0º). Equivalent superpositions for bHsc70 with hHsp70 provide baselines of just 1.1, 1.4 and 1.4º, respectively.

Structure within Sse1 subdomains also differs appreciably from that in hHsp70 (Cα r.m.s.d.s of 1.08, 1.14, 1.35, and 0.76Å for IA, IB, IIA and IIB, respectively), more so than between DnaK and hHsp70 (0.85, 0.99, 0.87, 0.89Å, respectively) or between bHsc70 and hHsp70 (0.48, 0.25, 0.29, and 0.21Å, respectively). Sequence divergence accounts for much of this structural distinction (sequence identity with hHsp70 NBD: 33% for Sse1, 51% for DnaK, and 88% for bHsc70), but the impact of contacts from SBD to all but IIB must also contribute.

C. Comparison of ATP interactions in Sse1 and Hsp70s

ATP is intact in our structure of Sse1, whereas it was hydrolyzed to the products ADP and phosphate (P_i) in initial structures of bHsc70 and hHsp70 (Flaherty et al., 1990; Sriram et al., 1997). All subsequent structures remained in this ADP conformational state, including ones with ATP captured intact by mutationally disabled Hsc70s (Flaherty et al., 1994; O'Brien et al., 1996). Nevertheless, there is great similarity in nucleotide binding between Sse1(ATP) and bHsc70(ADP) and hHsp70(ADP) and the nucleotide-contacting residues have exceptionally high sequence conservation. Contacts with the adenine-ribose-α-phosphate moiety, all from lobe II, are virtually identical in each. The one substitution (Lys276

in Sse1 for Arg272 in Hsp70s) involves only aliphatic contacts. Interactions at the β- and γ-phosphate positions (P_β, P_γ) necessarily differ somewhat because of differing NBD conformations, but contacting residues are highly conserved (Asp8/10, Asn11/Thr13, Lys69/71, Asp174/Glu175, Asp203/199, Ser208/Thr204, and Thr210/Asp206 for Sse1/bHsc70).

We have compared Sse1(ATP) with the ATP-Mg^{2+}-K^+ complex with the NBD of K71M bHsc70 (O'Brien et al., 1996), a putative "precatalytic" state poised for in-line nucleophilic attack on P_γ (Flaherty et al., 1994; Johnson and McKay, 1999). The ATP conformations are the same in these two proteins, with Mg^{2+} coordinated in the same bidentate manner with positioning by Asp 8 and Asp203 as by 10 and 199 in bHsc70. (Fig. 3C). Sse1(ATP) binds K^+ as at bHsc70 site #1, but there is no other K^+ site as in bHsc70. More importantly, Lys69 and Asp174 are displaced from Hsc70-like positions due to the altered orientation for lobe I in Sse1. Lys69 and Asp174 do direct hydrogen-bonds to the ATP (to a P_γ oxygen and a Mg^{2+} water, respectively), but Lys69 adopts a rare rotameric state and neither residue is properly poised for its putative catalytic role. Catalysis by Hsc70 is highly sensitive to mutation at counterpart residues; k_{cat}/K_m is reduced ~1000-fold for E175Q and E175S (Wilbanks et al., 1994) and K71M/E/A are all totally devoid of ATPase activity (O'Brien et al., 1996). K69M Sse1 is also inactive (Raviol et al., 2006), and although mutational tests have not been reported on Asp174 in Sse1, it seems likely from the structure that its carboxylate will play the same catalytic role as Glu175 in Hsc70. The absence of ATP hydrolysis in this SBD-engaged, Lys69-displaced state of Sse1 is understandable.

D. Interlobe interfaces in Sse1(ATP) and hHsp70(ADP)

Interfaces between NBD lobes in Sse1 feature conformation-specifying interactions that also impact the ATP-binding site. The NBD conformation is such that the front-face cleft is widened in Sse1(ATP) relative to hHsp70(ADP) and that on the back side is narrowed (canonical view, Fig. 3A). A hydrogen-bonded triplet of residues bridges between subdomains IA and IIA in Sse1 on the front side, and another triplet between subdomains IB and IIB ties the back side together. Gln368 on IA hydrogen bonds to Arg346 on IIA and to neighboring Asp369 as well (Fig. S3**A**); and side-chain hydrogen bonds link Arg235 on IIB to both Asn67 and Glu84 on IB (Fig. S3**B**). Each of these interactions is specific to Sse1. In Hsp70s, Glu231 replaces Arg235 of Sse1 but it cannot be stabilizing (Fig. S3**B**), and Pro365 replaces Gln368 but it cannot be bridging. Invariant residues Arg342, Asn364 and Asp366 form an alternative hydrogen-bonded triple in hHsp70(ADP) (Fig. S3**A**).

The Arg235-Asn67-Glu84 triplet affects placement of the catalytic Lys69 in Sse1(ATP), both directly because of peptide linkage to Asn67 and indirectly through dual hydrogen bonds between Glu84 and Arg70, another Lys69 neighbor. Corresponding residues Asp86 and Arg72 make water-mediated hydrogen bonds in hHsp70(ADP), but there is no IIB linkage. Similarly, placement of the catalytic Asp174 in Sse1(ATP) is affected by the Arg346-Gln368-Asp369 triplet (and in Sse1(ADP) by a hypothetical Arg346-Asn367-Asp369 triplet). Nearby Ile372 on NBD helix O makes direct hydrophobic contacts to Cβ atoms of both Asp174 and Ala 178 on NBD helix G, while conserved Arg346 also makes aliphatic contacts in adenosine binding. At least in Sse1 then, observed displacements in catalytic residues correlate both with inter-lobe stabilizations and loss of hydrolytic activity. We find that the hHsp70(ADP) conformation is accessible to Sse1, provided that SBD is removed, and vice versa that hHsp70 should be able to adopt the Sse1(ATP) conformation. We judge from this modeling that a putative hHsp70(ATP)

conformation would have none of the three defining hydrogen bonds of Sse1(ATP) but that it would gain another (Arg72-Glu231).

Other interactions also control the relative disposition of subdomains near the catalytic center within Sse1(ATP) as compared with hHsp70(ADP). As noted by Vogel et al. (2006), the segment Pro146 to Arg154 (Sse1 numbering) is critical for catalytic activity, and hydrogen-bonding of both Pro146O – Asp174N and the guanidinium group of Arg154 with the side chain of Asn173 and the main-chain carbonyls at positions 148 and 150 in Sse1(ATP) are absolutely conserved in hHsp70(ADP) (Fig. S3**C**). This, in turn, positions the respective catalytic residues Asp174 (Glu175) and the aromatic residues Trp148 (Tyr149) and Tyr149 (Phe150) into comparable positions. In the case of Sse1(ATP), hydrogen bonds between Trp148 Nε and Ser208 Oγ and between Tyr149 Oη and Lys71 O then fix the relative position of ATP since Ser 208 also binds to the Pγ phosphate of ATP. Homologous Thr204, which binds to the Pi phosphate in hHsp70(ADP), is displaced by 4.3Å in hHsp70(ADP), but if moved to the Sse1(ATP) conformation its Oγ would then be in position to hydrogen bond to Tyr149 Oη. In this picture (Fig. S3C), the nucleotide in Sse1(ATP) is held back from the catalytic center by ~3Å relative to its position in hHsp70(ADP). Conserved hydrogen bonding between Arg70 and carbonyl 230 in Sse1 (Arg72 and carbonyl 226 in hHsp70) keeps subdomain IB positioned relative to IIA even as the guanidinium unit swings by ~4.8Å (Fig. S3D). Catalytic Lys69 in IB is also tied to IA through bridging hydrogen bonds provided by Gln153 in Sse1(ATP), but this joining is prized apart at the homologous Gln154 in hHsp70(ADP). Finally, we note that conserved Tyr182, two turns away from catalytic Asp174 on IA helix αG, hydrogen bonds to Arg197 in IIA in Sse1(ATP). This entails a conformational flip (χ1 trans to gauche minus) relative to hHsp70(ADP) whereby Oη moves 9.4Å from a main-chain interaction within IA in hHsp70(ADP).

Supplemental Text S5

Simulation of SAXS data from Sse1 atomic coordinates

Atomic coordinates from the structure of Sse1(ATP) protomer B were used to simulate the small-angle x-ray scattering (SAXS) expected from this structure in solution. This SAXS simulation was done with the program CRYSOL (Svergun, 1995) and resulting scattering profiles were analyzed with the GNOM program (Semenyuk, 1991) to deduce the pair-distribution function, P(r), radius-of-gyration, R_g, and maximal distance, d_{max}. This characterization of simulated SAXS information from Sse1(ATP) agrees remarkably well with that observed from bHsc70(ATP) (Wilbanks et al., 1995). Although these are different proteins (25.7% sequence identity) of somewhat different sizes (650 residues for bHsc70 and 554 residues for bHsc70ΔC vs. 625 residues in the Sse1 model, including 43 residues with side chains abbreviated to Cβ due to disorder and excluding a 23-residue acidic-loop insertion and a 41-residue C-terminal extension), their SAXS characteristics are similar. In each case, SAXS parameters computed from Sse1 are distinct from those of bHsc70 or bHsc70ΔC with ADP or nucleotide free.

The radius-of-gyration computed from the simulated P(r) for Sse1 (R_g = 31.4Å) is intermediate between those derived from the experimental P(r) distributions for bHsc70(ATP) and bHsc70ΔC(ATP) (averages of 34.6Å and 29.2Å, respectively), as is d_{max} (117Å vs. 120Å and 115Å, respectively). In contrast, the R_g from Sse1 is substantially smaller than those seen for either bHsc70(ADP) or bHsc70ΔC(ADP) (averages of 40.1Å and 34.3Å, respectively). Most importantly, the full P(r) distributions are

also similar to the bHsc70(ATP) distributions and decidedly different from bHsc70(ADP) distributions (Fig. S9).

Supplemental Experimental Procedures

Protein expression and purification

Sse1 proteins were produced in *E. coli* with the pSMT3-Ulp1 protease system (Mossessova and Lima, 2000). The full-length yeast *SSE1* gene was PCR-amplified from genomic *S. cerevisiae* DNA and various constructs were cloned into pSMT3 vectors through the *BamHI* and *XhoI* sites. Sse1 proteins were expressed in *E.coli* strain BL21(DE3) (Novagen) as Smt3 fusion proteins with N-terminal His6-tags on Smt3. Following affinity purification on a HisTrap column (GE Healthcare Life Sciences), Smt3 was removed using Ulp1 protease. Proteins were further purified by size-exclusion chromatography on a HiLoad 26/60 Superdex 200 column (GE Healthcare Life Sciences) and ion-exchange chromatography on a Mono Q HR 10/10 column (GE Healthcare Life Sciences). The pSMT3 vector-Ulp1 protease system was a generous gift from Dr. Chris Lima.

Cleavage by Ulp1 protease leaves an N-terminal Ser as a production artifact on the product protein (Mossessova and Lima, 2000). The product from cloning of the full-length *SSE1* into the pSMT3 vector then yields the N-terminal amino-acid sequence SMSTP...., and we label this product as Sse1(-1-693). We also made a construct such that the artifactual Ser would correspond to Ser2 of the natural Sse1, and we label this product as Sse1(2-693). Sse1(2-659) was designed to terminate in correspondence with the SBD construct of DnaK for which structures were determined (Zhu et al., 1996). Selenomethionyl Sse1(2-659) was produced with the autoinduction procedure of Studier (2005). Predicted size and complete Se incorporation were confirmed by mass spectrometry.

Crystallization, data collection and model building

Sse1(2-659) crystals were grown by hanging-drop vapor diffusion at 20ºC by mixing protein solution (~10 mg/ml, in a buffer containing 10 mM Hepes-KOH pH7.0, 20 mM KCl, 10 mM $Mg(OAc)_2$ and 4 mM ATP) with a reservoir solution composed of 0.1M cacodylate-HCl (pH6.5) and 8-10% PEG6000. Single crystals were obtained by streak seeding. Native and selenomethionyl (SeMet) crystals grew under similar conditions. Single crystals grew as diamond-shaped plates (typically ~50μ on a side x ~10μ thick, but as large as 200μ x 40μ). Before freezing in liquid nitrogen, crystals were cryoprotected by soaking in 0.1M cacodylate-HCl (pH6.5), 8-10% PEG6000 and 20% glycerol. The crystals belong to the space group C2 (a=218.05Å, b=125.33Å, c=74.71 Å and β=98.7º) and have two Sse1(2-659) molecules per asymmetric unit.

X-ray diffraction data sets were collected at NSLS beamline X4A and processed with HKL2000 (http://www.hkl-xray.com (Otwinowski, 1997)). Phases were evaluated from multiwavelength anomalous diffraction (MAD) measurements (Hendrickson, 1991) using a three-wavelength data set from a SeMet crystal. Optimal wavelengths were determined by scanning selenomethionine dissolved in 0.1 M MES-NaOH pH6.5 and 10 % PEG6000 since As atoms in the cacodylate buffer absorb the fluorescence of Se. The program SOLVE (Terwilliger and Berendzen, 1999) was used to determine Se sites and initial phases at 3Å resolution. These phases were then transferred to the 2.4Å SeMet data set from a larger crystal, and these data were submitted to both RESOLVE (Terwilliger, 2000) and Arp/wArp (Perrakis et al., 1999) for phase extension and model building. An initial model was automatically built by

Arp/wArp, and the map produced with RESOLVE phases was used in subsequent manual rebuilding carried out with O (Jones et al., 1991). We used CNS (Brunger et al., 1998) for initial refinement and REFMAC (CCP4, 1994) in the final stages, all against the 2.4Å data.

Site-directed mutagenesis and growth tests

All site-directed mutants were constructed using the QuikChange Site-Directed Mutagenesis Kit (Stratagene, La Jolla, CA 92037). For testing the phenotype of *dnak* mutants, mutants were cloned into a *dnak* expression plasmid pBB46 (amp^R) and transformed into a *Δdnak* strain BB205 (cam^R kan^R) (Burkholder et al., 1996). Transformants were selected at 30ºC. Ten-fold dilutions of fresh 30ºC overnight cultures, which were inoculated from fresh transformants, were spotted on LB plates supplemented with 50 μg/ml ampicillin, 25 μg/ml kanamycin, 25 μg/ml chloramphenicol and 20 μg/ml IPTG. Growth was evaluated after one day incubation at 30ºC and 40ºC.

To test the phenotype of the *SSE1* mutants, a DNA fragment containing the promoter region and open reading frame of *SSE1* was amplified from yeast genomic DNA and cloned into plasmid pRS313 through the *BamHI* and *XhoI* sites. Mutants were introduced into pRS313-SSE1, and transformed into a *SSE1* deletion strain *YPL106C BY4742* (*MATα his3Δ1 leu2Δ0 lys2Δ0 ura3Δ0 trp1Δ1 ΔSSE1*) (ATCC).

The phenotypes of *SSA1* mutants were tested in yeast strain *JB67* (*MATα leu2-3,112 his3-11 ura3-52 trp1Δ1 lys2 ssa1-45:URA3 ssa2::LEU2 ssa3::TRP1 ssa4::LYS2*) (Becker et al., 1996). *ssa1-45* carries a single amino acid alteration P417L, which results in temperature-sensitive phenotype at 37ºC when *SSA2*, *SSA3* and *SSA4* are deleted. The *SSA1* mutants were introduced into plasmid pRS313-SSA1. Transformants were selected at 30ºC on yeast minimum media lacking histidine. Ten-fold dilutions of fresh overnight cultures for each transformant were spotted on yeast minimum media lacking histidine. Growth for *SSE1* mutants was tested at 30ºC and 40ºC for three overnights, and 30ºC and 37ºC for *SSA1* mutants.

The phenotypes of *SSC1* mutants were tested in yeast strain *QL1* (*pep4::HIS3 trp1-1 ssc1ΔCla*I::LEU2 pRS316-SSC1-URA3) (Liu et al., 2001). The *SSC1* mutants were introduced into plasmid pRS314-SSC1 (Miao et al., 1997). After transforming *QL1* with pRS314-SSC1-TRP1 containing mutant or WT versions of *SSC1*, transformants were selected at 30ºC on yeast minimum media lacking tryptophan. The phenotype of the *SSC1* mutants on pRS314-SSC1 was tested by spotting ten-fold dilutions of fresh overnight cultures on 5-fluoroorotic acid (5-FOA) plates, which only allow cells lacking pRS316-SSC1 to grow. Growth was scored at 30ºC and 37ºC for three overnights using growth on yeast plates lacking tryptophan as a control.

Western blot analysis of mutant expression

For testing the expression level of DnaK mutants, fresh overnight cultures were inoculated from fresh transformants and grown at 30ºC in LB supplemented with 50 μg/ml ampicillin, 25 μg/ml kanamycin, 25 μg/ml chloramphenicol. 50-fold dilutions were further grown at 30ºC for 4-5 hours in the presence of 20 μg/ml IPTG. 0.8 O.D. culture was collected, pelletted and resuspended in 200 μl SDS-SB. 5 μl was loaded on SDS-PAGE and Western blotting analysis was performed with anti-DnaK antibody mAb (E82/2) (Calbiochem).

For testing the expression level of Sse1 mutants, fresh overnight cultures were diluted 30 fold in yeast minimum media lacking histidine to allow further growth at 30ºC for another 4-5 hours. 2 O.D. cultures were collected, pelletted and resuspended in 50μl PBS buffer (16 mM Na_2HPO_4, 4 mM NaH_2PO_4, 150 mM NaCl and 1mM PMSF). 60 μl SDS-Triton (2% SDS and 0.2% Triton X-100) and ~30 μl acid-washed glass beads were added. A 2-min vortex was applied to

break open yeast. After adding 120 μl 2XSDS sample buffer, 5μl was loaded on SDS-PAGE and Western blotting analysis was performed with an anti-Sse1 antibody generated by Custom Polyclonal Antibody Production (Invitrogen).

Protein translocation in yeast

Transformed yeast strains harboring wild-type and mutant Ssa1 or Sse1 were grown overnight at 28°C in yeast minimum media lacking histidine. The fresh overnight cultures were diluted to O.D.=0.2, and further grown at 25°C for another 4-5 hours to reach mid-log phase (O.D.= 0.5 to 1.0). The cultures were then shifted to 33°C for 30 min to induce ppαF accumulation in the vector control and many mutants. Several temperatures were tested and 33°C was chosen due to the biggest difference between the wild-type and vector control. 2 O.D. samples were harvested and washed with ice-cold water. The cell pellets were resuspended in 25μl PBS buffer. 30 μl SDS-Triton and ~15 μl acid-washed glass beads were added. Then, a 2-min vortex was applied to break open yeast. After adding 15 μl 5XSDS sample buffer, 10μl was loaded on 15% SDS-PAGE and Western blotting analysis was performed with an anti-ppαF antibody at 1:1000 dilution (obtained from R. Schekman, UC, Berkeley). Anti-phosphoglycerate kinase (PGK) monoclonal antibody (Molecular Probes, Inc., Eugene, OR) was used at 1:2000 dilution as loading control.

Protein aggregation in *E.coli*

To test the ability of the DnaK mutants to prevent protein aggregation after heat-shock (42°C), the DnaK mutants on plasmid pBB46 were transformed into the *Δdnak* strain BB205 (*cam*^{R} *kan*^{R}) as described above. Fresh overnight cultures of the wild-type and mutant cells were grown at 30°C in LB supplemented with 50 μg/ml ampicillin, 25 μg/ml kanamycin, 25 μg/ml chloramphenicol. 100-fold dilution was further grown at 30°C for 3 hours in the presence of 20 μg/ml IPTG to reach 0.6 O.D. The cultures were shifted to 42°C in shaking water bath for 1 hour followed by another hour of incubation at 30°C. Cultures were cooled rapidly in an ice–water bath for 10 min, then 10 ml aliquots were centrifuged for 10 min at 5,000 *g* and 4°C to harvest the cells. Pellets were resuspended in 10X lysis buffer (100 mM Tris–HCl pH 7.5, 100 mM KCl, 2 mM EDTA, 15% (w/v) sucrose, 0.5 mg/ml lysozyme) based on their optical density (50 μl lysis buffer per 10 ml culture of OD_{600}=1) and frozen at –80°C. These samples were then thawed slowly on ice. A 10 volume of ice-cold 1M guanidine hydrochloride was added and mixed by pipetting. To break open cells and shear DNA, a one-minute sonication was applied while cooling. Intact cells were removed by centrifugation at 2,000 *g* for 15 min at 4°C. The insoluble cell fraction was isolated by centrifugation at 15, 000 *g* for 15 min at 4°C. Pellets (the insoluble fractions) were washed twice with ice-cold water and analyzed by 4-15% SDS-PAGE followed by staining with Coomassie Brilliant Blue.

Limited proteolysis

Sse1 (2-659) was diluted into buffer containing 20 mM Hepes-KOH (pH7.0), 100mM KCl and 10 mM $Mg(OAC)_2$ with 1mM ATP, ADP, AMP-PNP or no nucleotide to final concentration 1 mg/ml. 9 μl Sse1 (2-659) was incubated with 1 μl trypsin (1ng/μl and 4ng/μl) at 20ºC for 30 min. For SDS-PAGE, SDS-sample buffer was added to stop the digest. For mass spectrometry, an equal volume of TFC (trifluoracetic acid) was added to stop trypsin digest. N-terminal sequencing was applied to digested bands separated by SDS-PAGE after

transferred to PDVF membrane. N-terminal sequencing and mass spectrometry were performed at the Columbia Biopolymers Core Facility.

Sequence and structure analyses

Sequence alignments were made with ClustalW (http://www.ebi.ac.uk/clustalw/ (Thompson et al., 1994)). Structural superpositions were made with TOSS (Hendrickson, 1979) and LSQKAB (Kabsch, 1976)). Secondary structure assignments were made with DSSP (Kabsch and Sander, 1983) and VMD (http://www.ks.uiuc.edu/Research/vmd/ (Humphrey et al., 1996)). The Ramachandran analysis was made with MolProbity (http://kinemage.biochem. duke.edu (Lovell et al., 2003)).

Illustrations

Figures were generated using Molscript (http://www.avatar.se/molscript/ (Kraulis, 1991)), VMD (Humphrey et al., 1996), Grasp (Nicholls et al., 1991), ConSurf (http://consurf.tau.ac.il/ (Landau et al., 2005)), and PowerPoint.

Supplemental References

Becker, J., Walter, W., Yan, W., and Craig, E.A. (1996). Functional interaction of cytosolic Hsp70 and a DnaJ-related protein, Ydj1p, in protein translocation in vivo. Mol. Cell. Biol. *16*, 4378-4386.

Brunger, A.T., Adams, P.D., Clore, G.M., DeLano, W.L., Gros, P., Grosse-Kunstleve, R. W., Jiang, J.S., Kuszewski, J., Nilges, M., Pannu, N.S., *et al.* (1998). Crystallography & NMR system: A new software suite for macromolecular structure determination. Acta Crystallogr. D *54*, 905-921.

Buchberger, A., Theyssen, H., Schroder, H., McCarty, J.S., Virgallita, G., Milkereit, P., Reinstein, J., and Bukau, B. (1995). Nucleotide-induced conformational changes in the ATPase and substrate binding domains of the DnaK chaperone provide evidence for interdomain communication. J. Biol. Chem. *270*, 16903-16910.

Burkholder, W.F., Zhao, X., Zhu, X., Hendrickson, W.A., Gragerov, A., and Gottesman, M.E. (1996). Mutations in the C-terminal fragment of DnaK affecting peptide binding. Proc. Natl. Acad. Sci. U S A *93*, 10632-10637.

CCP4 (1994). The CCP4 suite: programs for protein crystallography. Acta Crystallogr. D *50*, 760-763.

Cupp-Vickery, J.R., Peterson, J.C., Ta, D.T., and Vickery, L.E. (2004). Crystal structure of the molecular chaperone HscA substrate binding domain complexed with the IscU recognition peptide ELPPVKIHC. J. Mol. Biol. *342*, 1265-1278.

Flaherty, K.M., DeLuca-Flaherty, C., and McKay, D.B. (1990). Three-dimensional structure of the ATPase fragment of a 70K heat-shock cognate protein. Nature *346*, 623-628.

Flaherty, K.M., Wilbanks, S.M., DeLuca-Flaherty, C., and McKay, D.B. (1994). Structural basis of the 70-kilodalton heat shock cognate protein ATP hydrolytic activity. II. Structure of the active site with ADP or ATP bound to wild type and mutant ATPase fragment. J. Biol. Chem. *269*, 12899-12907.

Harrison, C.J., Hayer-Hartl, M., Di Liberto, M., Hartl, F., and Kuriyan, J. (1997). Crystal structure of the nucleotide exchange factor GrpE bound to the ATPase domain of the molecular chaperone DnaK. Science *276*, 431-435.

Hendrickson, W.A. (1979). Transformations to optimize the superposition of similar structures. Acta Crystallogr. *A35*, 158-163.

Hendrickson, W.A. (1991). Determination of macromolecular structures from anomalous diffraction of synchrotron radiation. Science *254*, 51-58.

Humphrey, W., Dalke, A., and Schulten, K. (1996). VMD: visual molecular dynamics. J. Mol. Graph. *14*, 33-38, 27-38.

Jiang, J., Prasad, K., Lafer, E.M., and Sousa, R. (2005). Structural basis of interdomain communication in the Hsc70 chaperone. Mol. Cell *20*, 513-524.

Johnson, E.R., and McKay, D.B. (1999). Mapping the role of active site residues for transducing an ATP-induced conformational change in the bovine 70-kDa heat shock cognate protein. Biochemistry *38*, 10823-10830.
Jones, T.A., Zou, J. Y., Cowan, S.W., and Kjeldgaard, M. (1991). Improved methods for building protein models in electron density maps and the location of errors in these models. Acta Crystallogr. A *47*, 110-119.

Kabsch, W. (1976). A solution for the best rotation to relate two sets of vectors. Acta Crystallogr. *A32*, 922-923.

Kabsch, W., and Sander, C. (1983). Dictionary of protein secondary structure: pattern recognition of hydrogen-bonded and geometrical features. Biopolymers *22*, 2577-2637.

Kraulis, P.J. (1991). MOLSCRIPT: a program to produce both detailed and schematic plots of protein structures. J. Appl. Crystallogr. *24*, 946-950.

Landau, M., Mayrose, I., Rosenberg, Y., Glaser, F., Martz, E., Pupko, T., and Ben-Tal, N. (2005). ConSurf 2005: the projection of evolutionary conservation scores of residues on protein structures. Nucl. Acids Res. *33*, W299-302.

Liu, Q., Krzewska, J., Liberek, K., and Craig, E.A. (2001). Mitochondrial Hsp70 Ssc1: role in protein folding. J. Biol. Chem. *276*, 6112-6118.

Lovell, S.C., Davis, I.W., Arendall, W.B., 3rd, de Bakker, P.I., Word, J.M., Prisant, M.G., Richardson, J.S., and Richardson, D.C. (2003). Structure validation by Cα geometry: ϕ, ψ, and Cβ deviation. Proteins *50*, 437-450.

Miao, B., Davis, J.E., and Craig, E.A. (1997). Mge1 functions as a nucleotide release factor for Ssc1, a mitochondrial Hsp70 of Saccharomyces cerevisiae. J. Mol. Biol. *265*, 541-552.

Morshauser, R.C., Hu, W., Wang, H., Pang, Y., Flynn, G.C., and Zuiderweg, E.R. (1999). High-resolution solution structure of the 18 kDa substrate-binding domain of the mammalian chaperone protein Hsc70. J. Mol. Biol. *289*, 1387-1403.

Mossessova, E., and Lima, C.D. (2000). Ulp1-SUMO crystal structure and genetic analysis reveal conserved interactions and a regulatory element essential for cell growth in yeast. Mol. Cell *5*, 865-876.

Nicholls, A., Sharp, K.A., and Honig, B. (1991). Protein folding and association: insights from the interfacial and thermodynamic properties of hydrocarbons. Proteins *11*, 281-296.

O'Brien, M.C., Flaherty, K.M., and McKay, D.B. (1996). Lysine 71 of the chaperone protein Hsc70 is essential for ATP hydrolysis. J. Biol. Chem. *271*, 15874-15878.

Otwinowski, Z., and Minor, W. (1997). Processing of X-ray diffraction data collected in oscillation mode. Meth. Enzymol. *276*, 307-326.

Perrakis, A., Morris, R., and Lamzin, V.S. (1999). Automated protein model building combined with iterative structure refinement. Nat. Struct. Biol. *6*, 458-463.

Raviol, H., Bukau, B., and Mayer, M.P. (2006). Human and yeast Hsp110 chaperones exhibit functional differences. FEBS Lett. *580*, 168-174.

Semenyuk, A.V., and Svergun, D.I. (1991). GNOM - a program package for small-angle scattering data processing. J. Appl. Crystallogr. *24*, 537-540.

Shaner, L., Trott, A., Goeckeler, J.L., Brodsky, J. L., and Morano, K.A. (2004). The function of the yeast molecular chaperone Sse1 is mechanistically distinct from the closely related hsp70 family. J. Biol. Chem. *279*, 21992-22001.

Sondermann, H., Scheufler, C., Schneider, C., Hohfeld, J., Hartl, F.U., and Moarefi, I. (2001). Structure of a Bag/Hsc70 complex: convergent functional evolution of Hsp70 nucleotide exchange factors. Science *291*, 1553-1557.

Sriram, M., Osipiuk, J., Freeman, B., Morimoto, R., and Joachimiak, A. (1997). Human Hsp70 molecular chaperone binds two calcium ions within the ATPase domain. Structure *5*, 403-414.

Stevens, S.Y., Cai, S., Pellecchia, M., and Zuiderweg, E.R. (2003). The solution structure of the bacterial Hsp70 chaperone protein domain DnaK(393-507) in complex with the peptide NRLLLTG. Protein Sci. *12*, 2588-2596.

Studier, F.W. (2005). Protein production by auto-induction in high density shaking cultures. Prot. Expr. Purif. *41*, 207-234.

Svergun, D., Barberato, C., and Koch, M.H.J. (1995). CRYSOL - a Program to Evaluate X-ray Solution Scattering of Biological Macromolecules from Atomic Coordinates. J. Appl. Crystallogr. *28*, 768-773.

Terwilliger, T.C. (2000). Maximum-likelihood density modification. Acta Crystallogr. D *56*, 965-972.

Terwilliger, T.C., and Berendzen, J. (1999). Automated MAD and MIR structure solution. Acta Crystallogr. D *55*, 849-861.

Thompson, J.D., Higgins, D.G., and Gibson, T.J. (1994). CLUSTAL W: improving the sensitivity of progressive multiple sequence alignment through sequence weighting, position-specific gap penalties and weight matrix choice. Nucl. Acids Res. *22*, 4673-4680.

Vogel, M., Bukau, B., and Mayer, M.P. (2006). Allosteric regulation of Hsp70 chaperones by a proline switch. Mol. Cell *21*, 359-367.

Wang, H., Kurochkin, A.V., Pang, Y., Hu, W., Flynn, G.C., and Zuiderweg, E.R. (1998). NMR solution structure of the 21 kDa chaperone protein DnaK substrate binding domain: a preview of chaperone-protein interaction. Biochemistry *37*, 7929-7940.

Wilbanks, S.M., Chen, L., Tsuruta, H., Hodgson, K.O., and McKay, D.B. (1995). Solution small-angle X-ray scattering study of the molecular chaperone Hsc70 and its subfragments. Biochemistry *34*, 12095-12106.

Wilbanks, S.M., DeLuca-Flaherty, C., and McKay, D.B. (1994). Structural basis of the 70-kilodalton heat shock cognate protein ATP hydrolytic activity. I. Kinetic analyses of active site mutants. J. Biol. Chem. *269*, 12893-12898.

Wilbanks, S.M., and McKay, D.B. (1995). How potassium affects the activity of the molecular chaperone Hsc70. II. Potassium binds specifically in the ATPase active site. J. Biol. Chem. *270*, 2251-2257.

Zhu, X., Zhao, X., Burkholder, W.F., Gragerov, A., Ogata, C.M., Gottesman, M.E., and Hendrickson, W.A. (1996). Structural analysis of substrate binding by the molecular chaperone DnaK. Science *272*, 1606-1614.

Table S1. Structural Comparison of Protomers in the Sse1 Dimer

	R.m.s.Deviation (Å)		Average B factor (Å^2)	
	Cα	All atom	Protomer A	Protomer B
Overall	0.43	0.64	57.8	47.9
NBD	0.23	0.49	55.1	44.0
IA	0.29	0.50	55.0	44.6
IIA	0.11	0.39	54.0	44.7
IB	0.21	0.61	56.9	43.0
IIB	0.11	0.36	54.1	43.6
SBD	0.58	0.82	62.3	54.1
β	0.45	0.71	64.3	57.1
α	0.60	0.84	60.5	51.1
ATP		0.12	39.2	28.2
Mg^{++}			45.4	28.8
K^{+}			48.0	36.6

Table S2. Buried surface area and shape complementarity on the interfaces

	Sse1		bHsc70ΔC	
	Buried surface area (Å^2)	Shape complementarity	Buried surface area (Å^2)	Shape complementarity
Linker-rest	1407	0.730	653	0.583
Linker-NBD	1196	0.734	449	0.581
Linker-SBD	255	0.802	194	0.587
NBD-SBD	2594	0.684	1045	0.415
NBD-SBDβ	1427	0.667	308	0.283
NBD-SBDα	1216	0.705	772	0.495
Dimer interface	1976	0.471		
NBD-NBD'	562	0.522		
NBD-SBD'	1448	0.456		
NBD(A)-SBD(B)	734	0.437		
NBD(B)-SBD(A)	714	0.475		

Sse1: NBD, 3-385; Linker, 386-396; SBD, 397-652; SBDβ, 397-540; SBDα, 541-652. bHsc70ΔC: NBD, 1-382; Linker, 383-395; SBD, 396-554; SBDβ, 396-507; SBDα, 508-554.

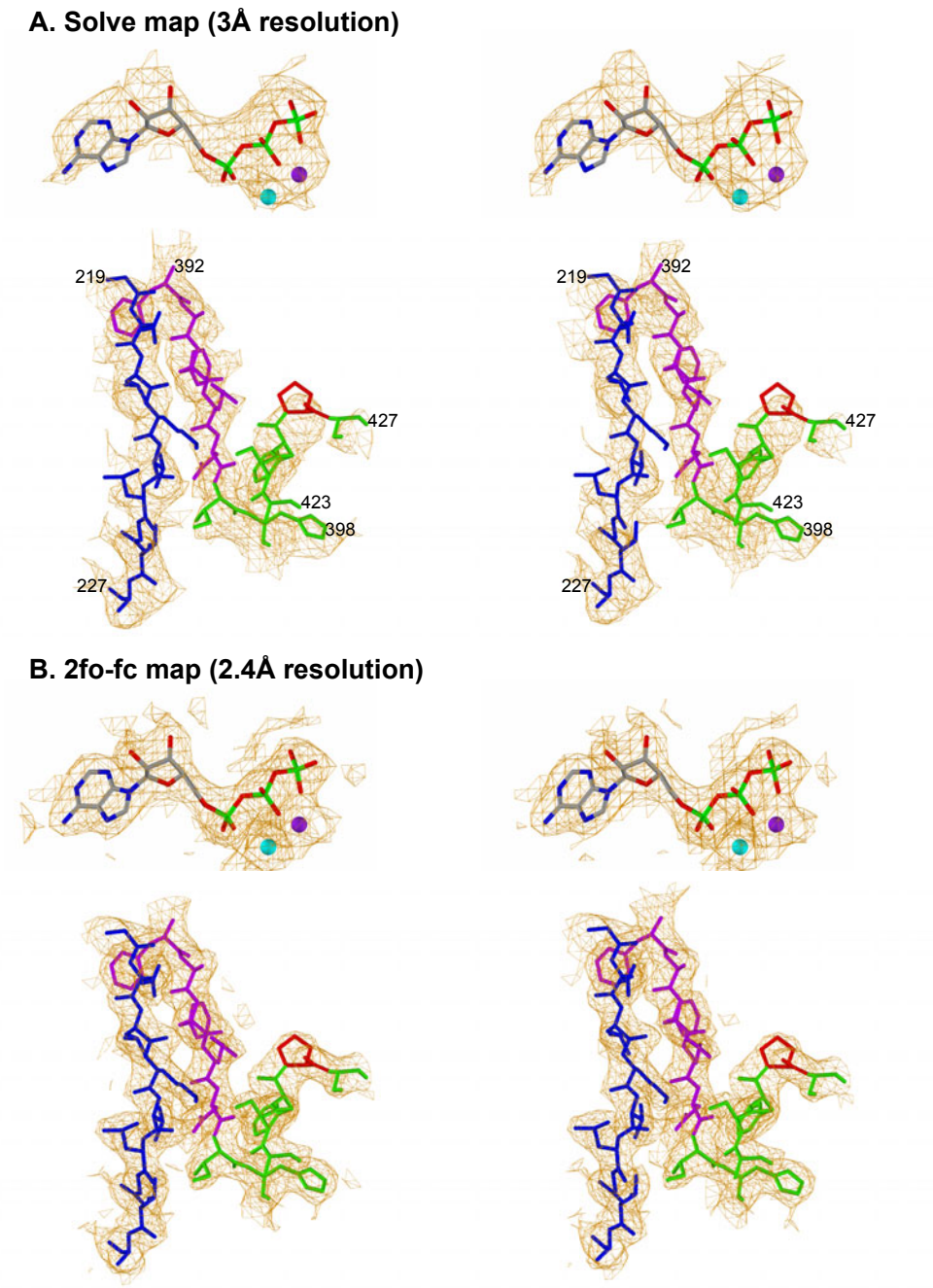

Figure S1. Electron-density distributions
(A) MAD-phased experimental map at 3.0Å resolution produced with SOLVE phasing parameters. **(B)** Model-phased (2|Fo| - |Fc|) map after refinement at 2.4Å resolution. Maps were produced using the FFT from CCP4 (1994) and drawn as 3D baskets contoured at the 1σ level using the 'covering' option in Molscript (Kraulis, 1991) to portray density associated with the selected atomic elements. ATP and associated Mg^{2+} and K^{+} ions (above) are shown colored as in Fig. **3C**. Portions of the inter-domain β-sheet (below) include NBD residues 219GQLKVLGTA227 (blue), linker residues 392FKFED396 (purple), and SBD residues 397IH398 and 423SSFPS427 (green). Lys393 is truncated at Cα due to lack of density and cis Pro426 is shown in red.

Figure S2

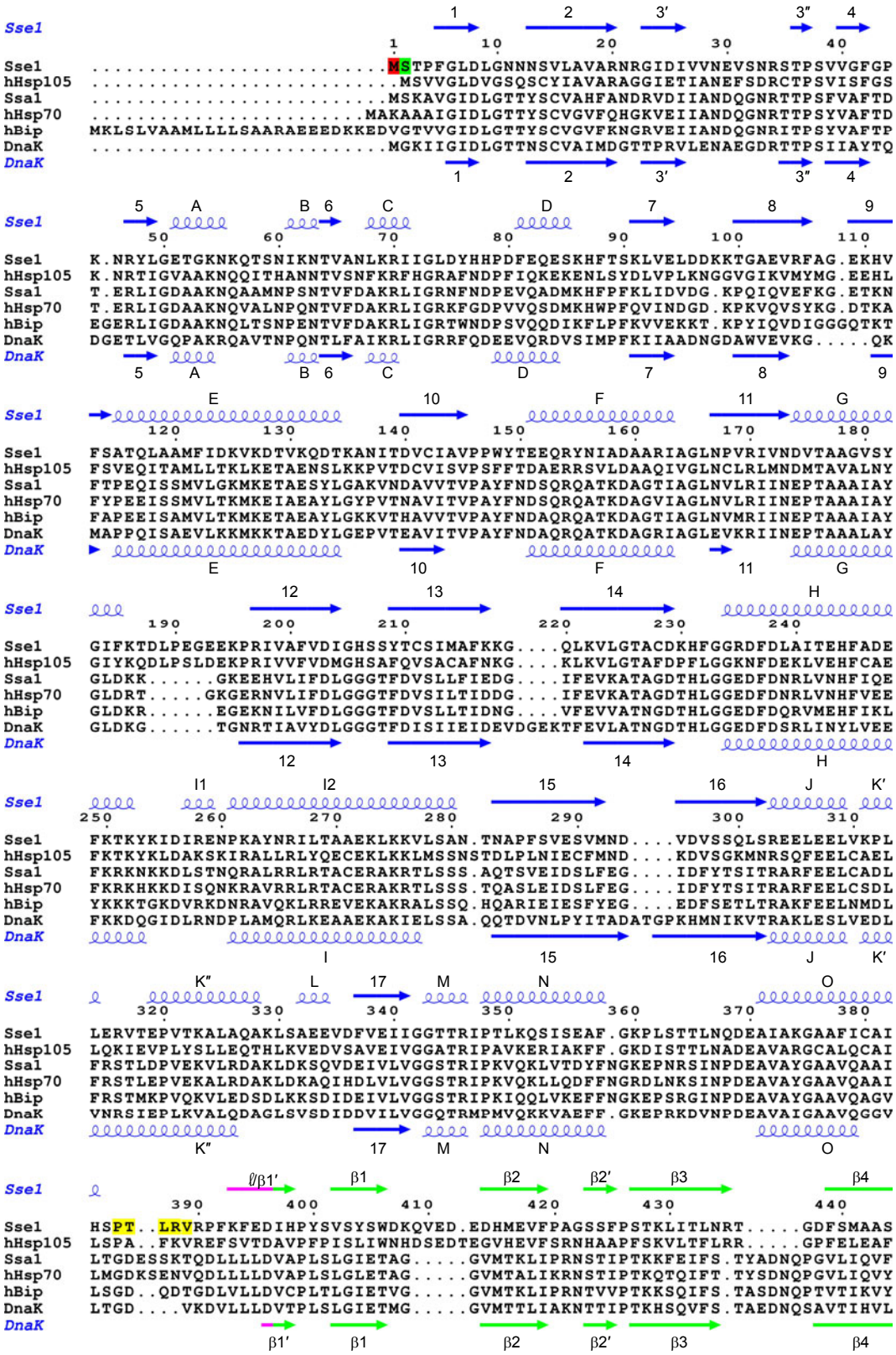

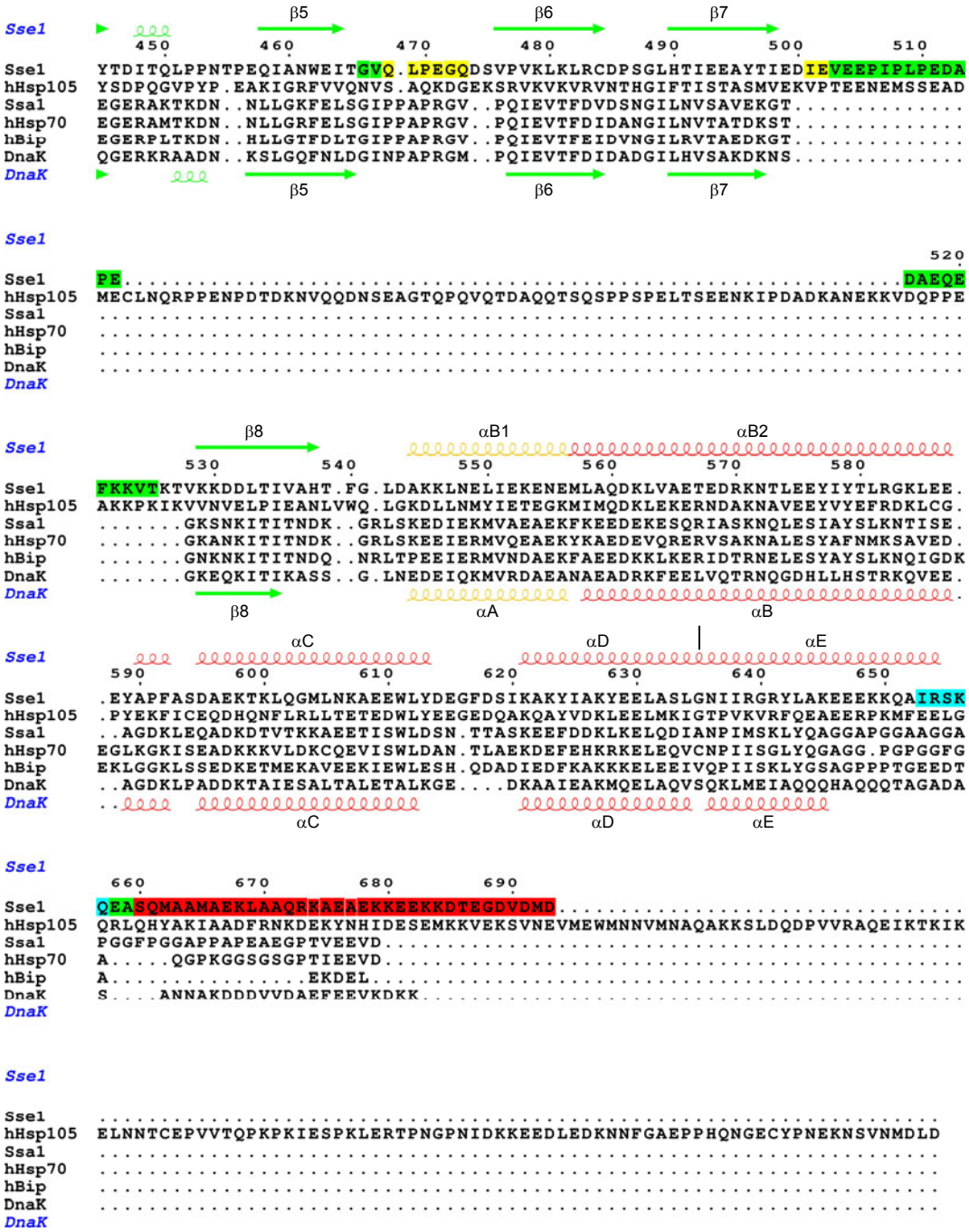

Subdomains of Sse1

NBD	IA	1-37 115-187 364-385
	IB	38-114
	IIA	188-232 311-363
	IIB	233-310
Interdomain linker		386-396
SBD	β	397-540
	α	541-657

Figure S2. Structure-based sequence alignment

Elements of secondary structure are specified and labeled for Sse1 (above) and for DnaK (below) based on DSSP (Kabsch and Sander, 1983) assignments for Sse1 and DnaK NBD (PDB 1DKG, (Harrison et al., 1997)) and as specified (Zhu et al., 1996) for DnaK SBD (PDB 1DKX). Sse1 residues that have highlighting are colored in the code: not cloned into the Sse1(2-659) construct (red), not ordered in either protomer (green), ordered in protomer A but not in B (blue), ordered in protomer B but not in A (yellow).

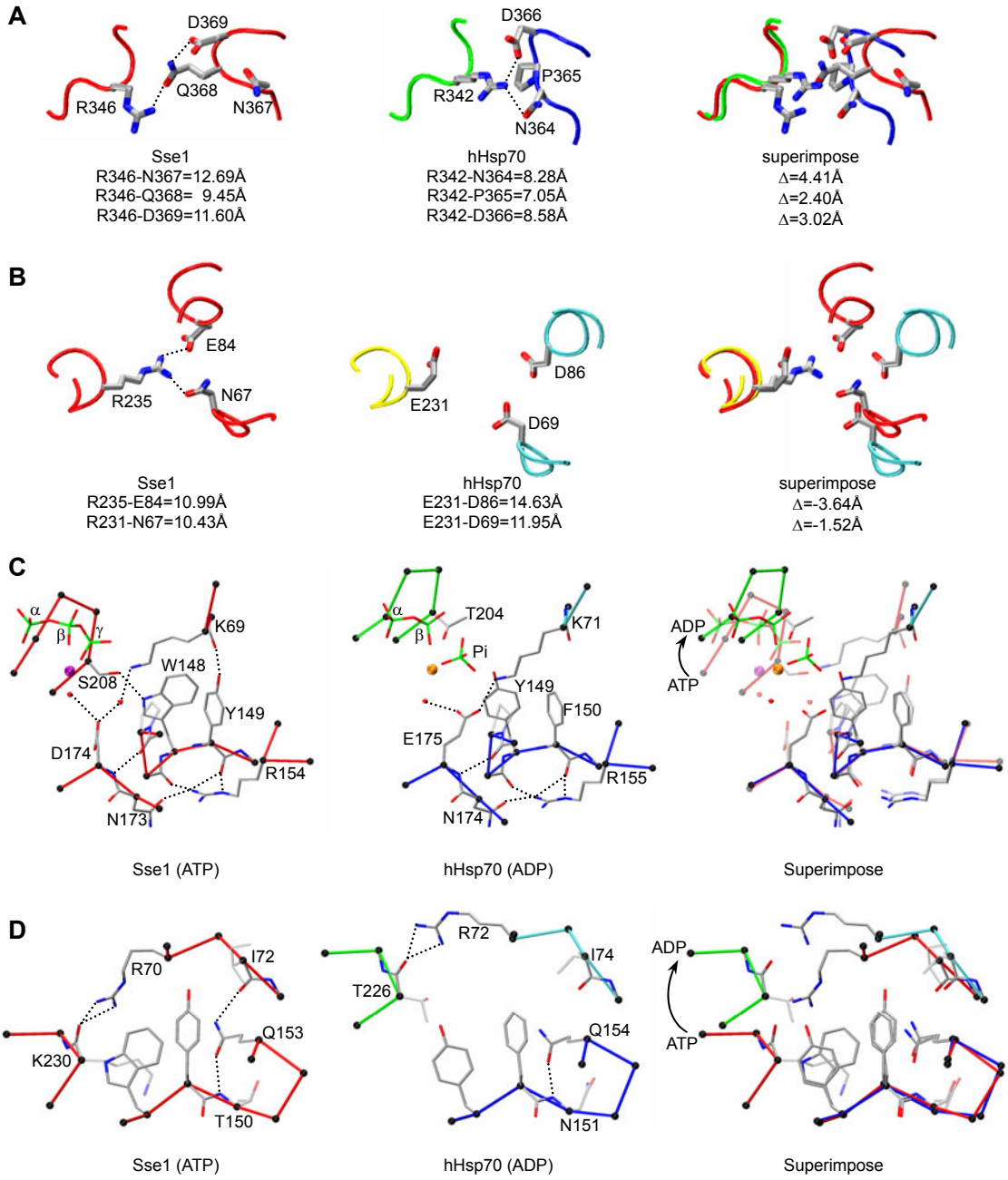

Figure S3. Comparison of NBD conformations in Sse1 and Hsp70s

Coloring for side-chain atoms has the pattern: carbon (grey), nitrogen (blue), oxygen (red); and that for backbone traces is Sse1 (red) with hHsp70 subdomains IA (blue), IB (cyan), IIA (green) and IIB (yellow) as in Fig. 3**B**. Hydrogen bonds are represented by black dotted lines. (**A**) Detail of hydrogen-bonded triplet at the IA/IIA interface in Sse1(ATP) (left) and the counterpart in hHsp70(ADP) (middle). The superposition (right) is based on IIA Cα atoms as in Fig. 3**B** (left) and the orientation is as in Fig. 3**A**. (**B**) Detail of hydrogen-bonded triplets at the IB/IIB interfaces in Sse1(ATP) (left) and hHsp70(ADP) (middle). The superposition (right) is based on IIB Cα atoms as in Fig. 3**B** (right) and orientation is also as in Fig. 3**B** (right). (**C**) Detail comparing subdomain dispositions near the catalytic center in Sse1(ATP) (left) and hHsp70(ADP) (middle). Oε1 and Nε2 of Q154 were exchanged from PDB assignments for H bonding. The superposition (right) is based on IA Cα atoms. Coloring is as for S3A with the addition of phosphate and ion atoms: phosphorous (green), oxygen (red), Mg^{2+} (purple), Ca^{2+} (orange). The orientation is approximately as in Fig. 3**C**. (**D**) Detail comparing additional interactions between subdomains near the catalytic center in Sse1(ATP) (left) and hHsp79(ADP) (middle). The superposition (right) is again as in Fig. S3**C**. The orientation is rotated from S3C by ~30º, mainly about the horizontal axis.

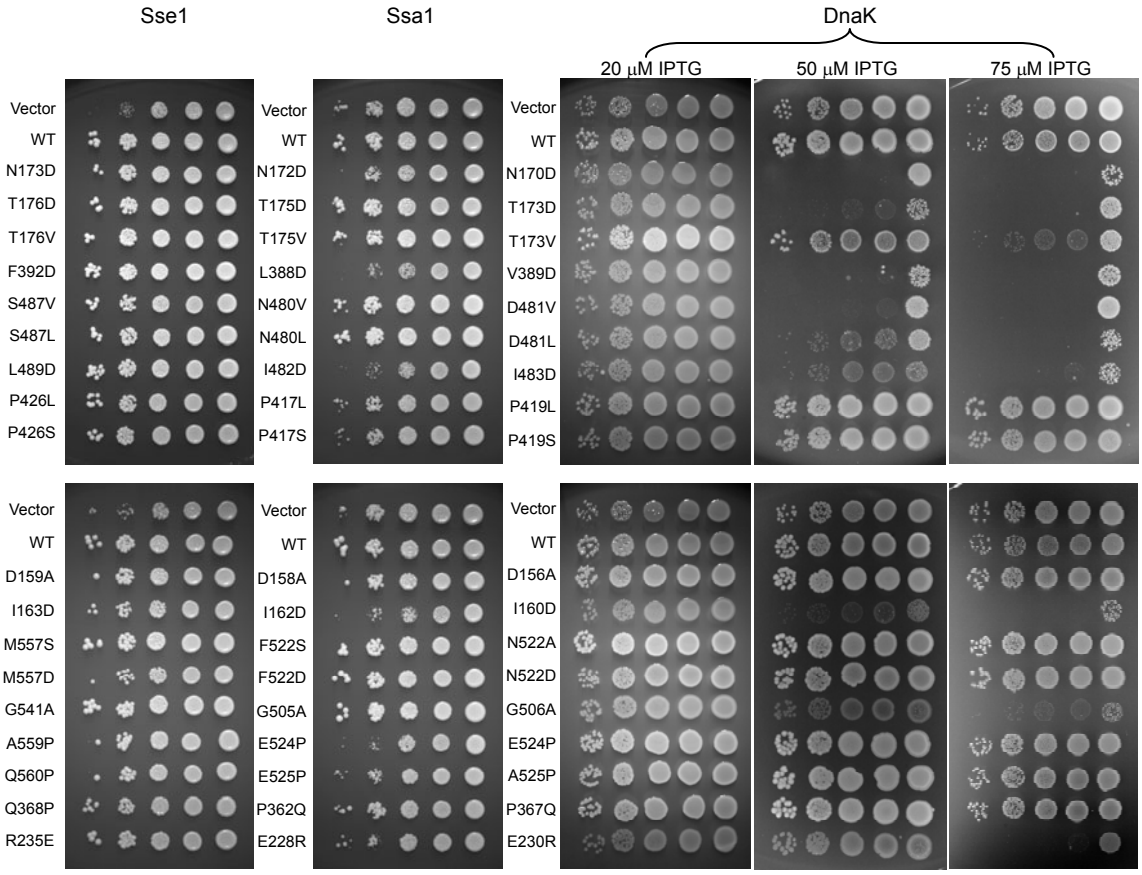

Figure S4. **Mutational analysis of mutants at the permissive temperature of 30°C**
Growth tests were performed as described in Fig. 5A except that the incubation temperature was 30°C. DnaK mutants were also tested on plates containing 50 and 75 μM IPTG, which induce the overexpression of DnaK proteins (Burkholder et al., 1996).

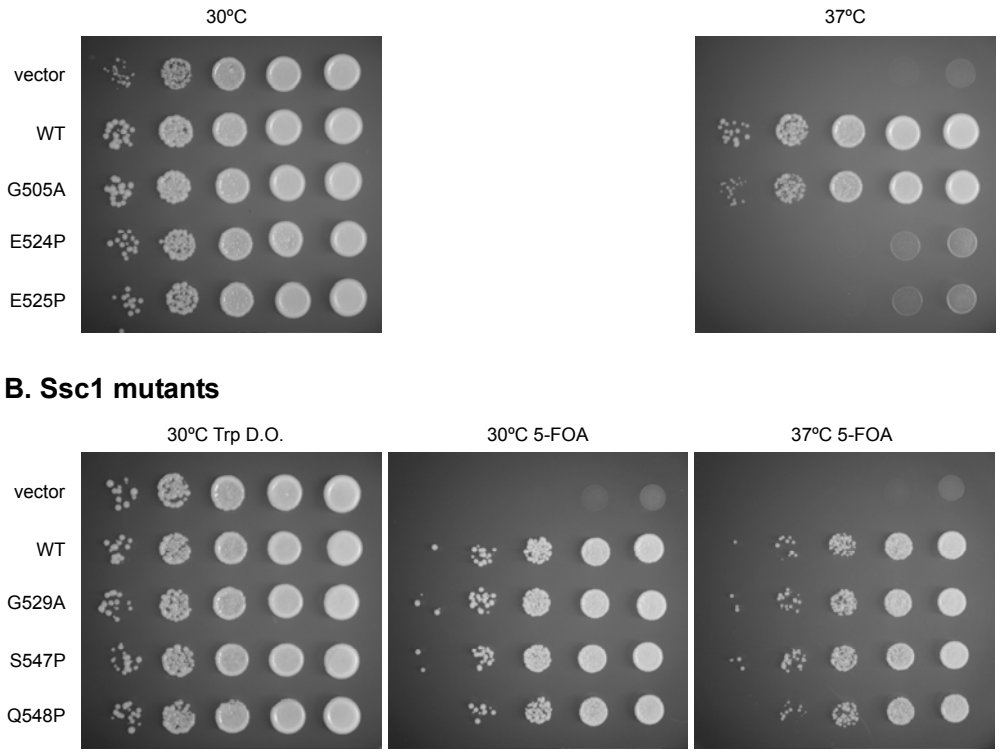

Figure S5. Mutational analysis of conformation-sensitive residues

(A) Tests of Ssa1 mutants. Growth tests were performed at 30°C and 37°C in the same temperature-sensitive *SSA1* background as described for Fig. **5**. **(B)** Tests of Ssc1 mutants. Mutant *SSC1* genes were introduced into a plasmid with a *TRP1* marker, and tested in a *ΔSSC1-ΔTRP1 S. cerevisiae* background that also contains a wild-type *SSC1* gene on a separate plasmid with a *URA3* marker (Liu et al., 2001). The wild-type *SSC1* plasmid is necessary since *ΔSSC1* is lethal. Growth was tested at 30°C on tryptophan drop-out (Trp d.o.) plates as a negative control to show that each strain was diluted to a similar level, and at 30°C and 37°C on 5-fluoroorotic acid (5-FOA) plates, which eliminate growth from the wild-type *SSC1* plasmid by inhibiting the *URA3* gene product tied to Ssc1 expression.

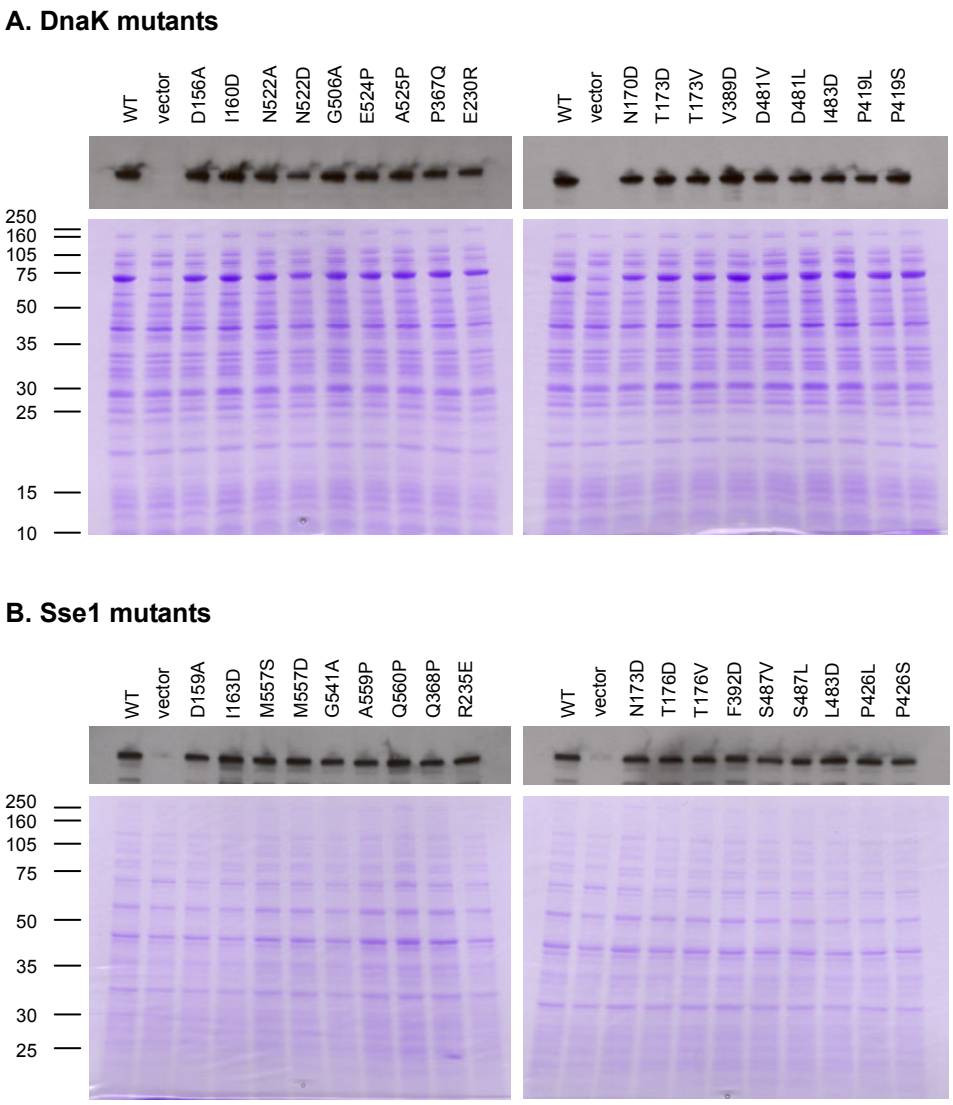

Figure S6. Protein expression levels for mutant proteins

(A) DnaK mutants. **(B)** Sse1 mutants. The bottom frames are of Coomassie-stained SDS-PAGE gels of the respective cell lysates, and the top frames are excerpts from Western blots with anti-DnaK (~70kD) and anti-Sse1 (~77kD) antibodies in the respective cases. All DnaK and Sse1 mutants are expressed at close to wild-type level. The use of a temperature-sensitive Ssa1 background precluded a similar assay of expression for the Ssa1 mutants.

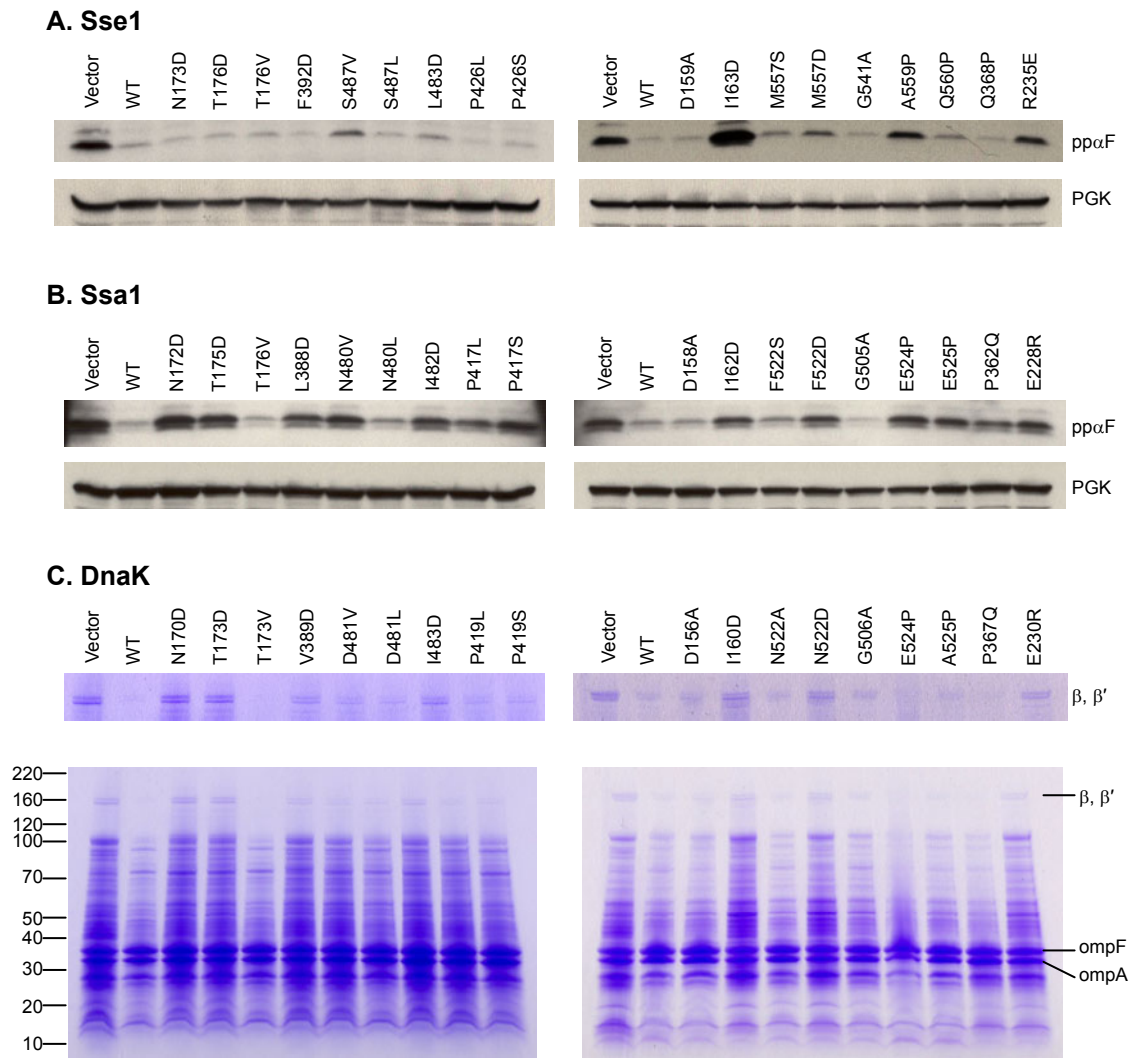

Figure S7. ppαF accumulation in Sse1 and Ssa1 mutants and protein aggregation in DnaK mutants

(A) Sse1 mutants. The top blots show the level of ppαF, while the bottom blots show the level of PGK as loading control. **(B)** Ssa1 mutants. The top blots show the level of ppαF, while the bottom blots show the level of PGK as loading control. **(C)** DnaK mutants. The top gels are ~150 kD excerpts of the corresponding bottom gels to show the aggregation of the β and β' subunits of RNA polymerase, which is labeled as β, β'. The bottom gels show the full-range of protein aggregation with the outer membrane protein ompF and ompA as loading controls. Molecular weight markers are labeled on the left.

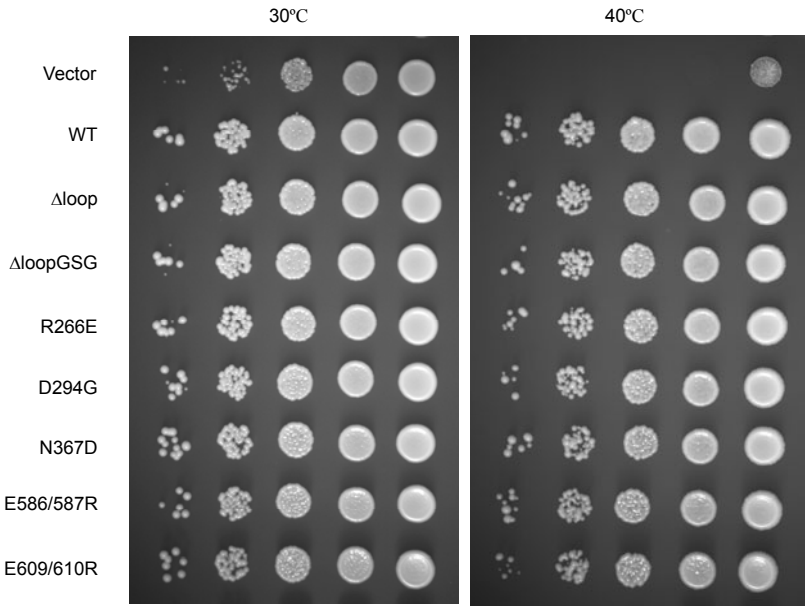

Figure S8. **Mutational analysis of dimer-interface and acidic-loop residues in Sse1**
Growth tests were performed at 30°C and 40°C as for the other Sse1 mutations described in Figs. **5** and **S4**.

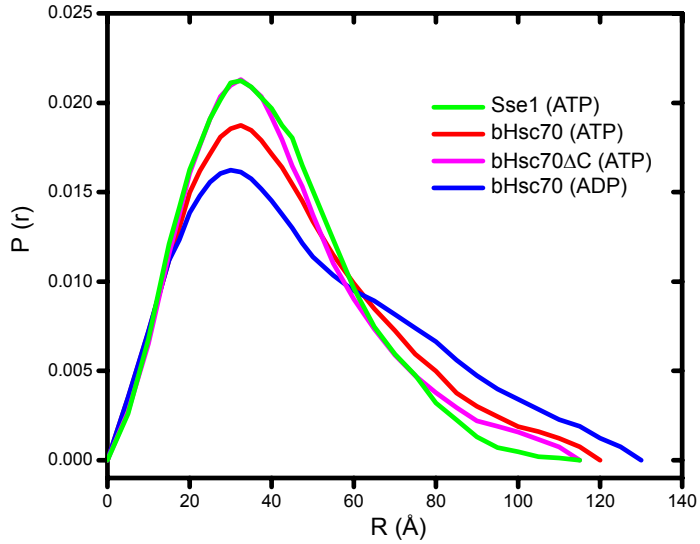

Figure S9. Comparison of the pair-distribution function simulated for Sse1(ATP) with those derived from SAXS data on bHsc70

The distribution for Sse1(ATP) was simulated with CRYSOL (Svergun, 1995) and GNOM (Semenyuk, 1991) from the atomic model, and then normalized to unit integrated probability. The bHsc70 distibutions were digitized from Figs. 4 and 7 of Wilbanks et al. (1995). The Sse1(ATP) distribution is drawn in green (R_g=31.4Å, d_{max}=117Å), bHsc70(ATP) is in red (R_g=34.6Å, d_{max}=120Å), bHsc70ΔC(ATP) is in magenta (R_g=29.2Å, d_{max}=115Å), and bHsc70(ADP) is in blue (R_g=40.1Å, d_{max}=130Å).

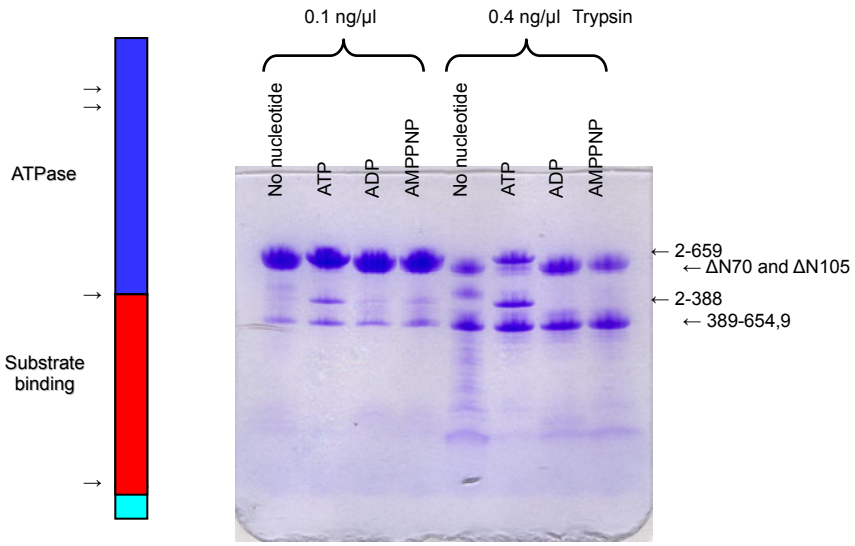

Figure S10. Nucleotide-dependence of proteolytic susceptibility

The Coomassie-stained SDS PAGE gel shows digestion profiles after 30 min. in trypsin at the indicated concentrations in the presence of no nucleotide, ATP, ADP and AMPPNP, as indicated.

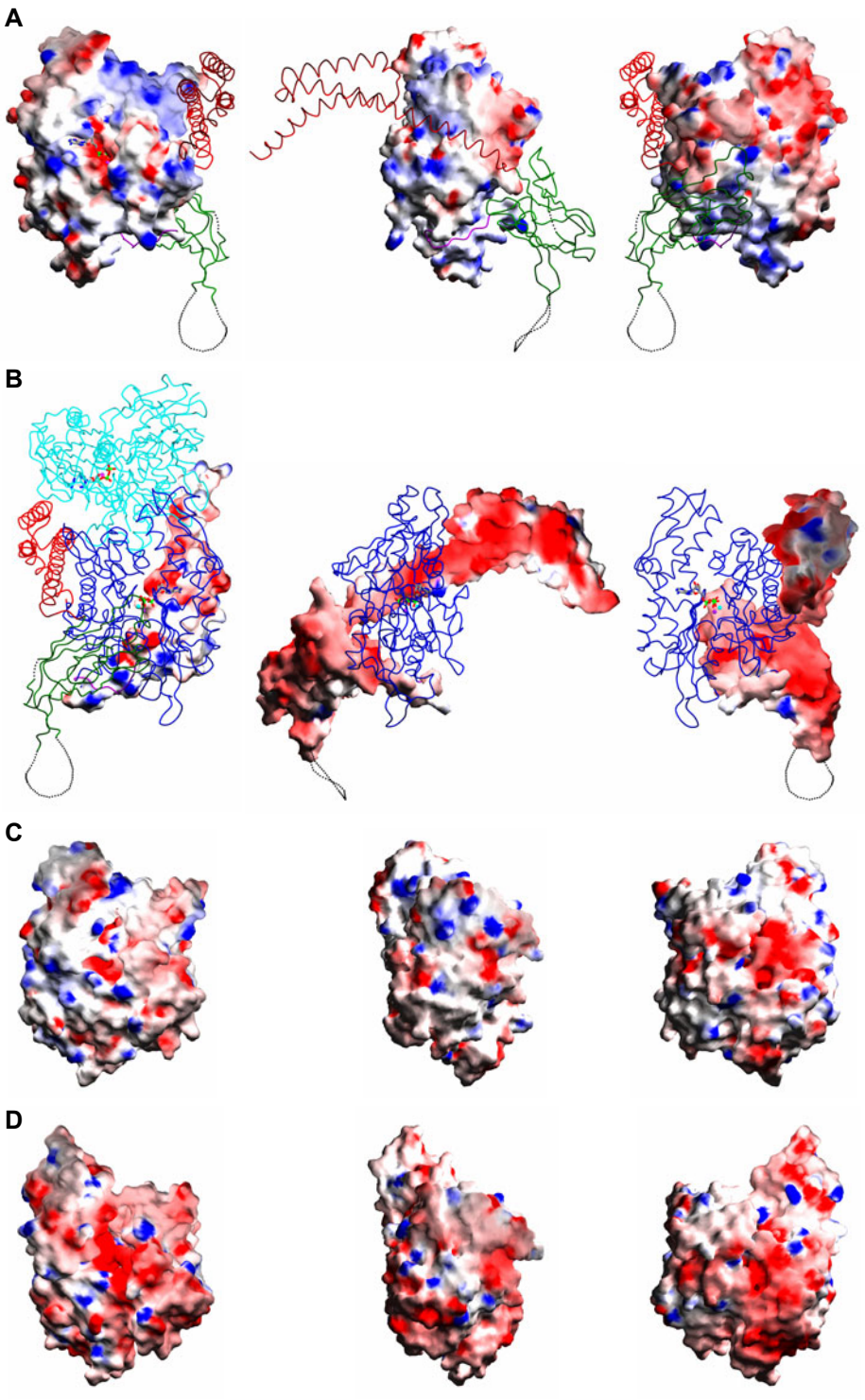

Figure S11. Electrostatic potential surfaces
(A) Mapping of electrostatic potential onto the surface of the Sse1 NBD in three orthogonal views as in Figs. 5 **A-C**. **(B)** Mapping of the electrostatic potential onto SBD surfaces of Sse1. Each frame is viewed 180º about the vertical from the respective frames in **A**, and partner Cα backbones are overlayed and color coded: NBD (blue), SBDβ (green), SBDα (red), and non-interacting elements of the protomeric mate (cyan). **(C)** Mapping of electrostatic potential onto the surface of the hHsp70 NBD as superimposed onto Sse1 oriented as in **A**. **(D)** Mapping of electrostatic potential onto the surface of the DnaK NBD as superimposed onto Sse1 oriented as in **A**. In each case, electrostatic potential is colored in increasing intensities of red for negative and blue for positive, with white remaining neutral (hydrophobic).